



**HAL**  
open science

## Calculation of electron interaction models in N<sub>2</sub> and O<sub>2</sub>

F. Nicolanti, B. Caccia, A. Cartoni, D. Emfietzoglou, R. Faccini, S. Incerti, I. Kyriakou, M. Satta, H.N. Tran, C. Mancini-Terracciano

### ► To cite this version:

F. Nicolanti, B. Caccia, A. Cartoni, D. Emfietzoglou, R. Faccini, et al.. Calculation of electron interaction models in N<sub>2</sub> and O<sub>2</sub>. *Physica Medica European Journal of Medical Physics*, 2023, 114, pp.102661. <10.1016/j.ejmp.2023.102661>. <hal-04202966>

**HAL Id: hal-04202966**

**<https://hal.science/hal-04202966v1>**

Submitted on 2 Oct 2023

**HAL** is a multi-disciplinary open access archive for the deposit and dissemination of scientific research documents, whether they are published or not. The documents may come from teaching and research institutions in France or abroad, or from public or private research centers.

L'archive ouverte pluridisciplinaire **HAL**, est destinée au dépôt et à la diffusion de documents scientifiques de niveau recherche, publiés ou non, émanant des établissements d'enseignement et de recherche français ou étrangers, des laboratoires publics ou privés.



HAL Authorization

# Calculation of electron interaction models in N<sub>2</sub> and O<sub>2</sub>

F. Nicolanti<sup>a,b,\*</sup>, B. Caccia<sup>c</sup>, A. Cartoni<sup>d</sup>, D. Emfietzoglou<sup>e</sup>, R. Faccini<sup>a,b</sup>, S. Incerti<sup>f</sup>,  
I. Kyriakou<sup>e</sup>, M. Satta<sup>d,g</sup>, H. N. Tran<sup>f</sup>, C. Mancini-Terracciano<sup>a,b</sup>

<sup>a</sup>*Physics Dep., Sapienza U. of Rome, p.le Aldo Moro, 5, 00185, Rome, Italy*

<sup>b</sup>*INFN, Sec. of Rome, p.le Aldo Moro, 2, 00185, Rome, Italy*

<sup>c</sup>*ISS(Italian National Institute of Health), V. Regina Elena, 299, 00161, Rome, Italy*

<sup>d</sup>*Chemistry Dep., Sapienza U. of Rome, p.le Aldo Moro, 5, 00185, Rome, Italy*

<sup>e</sup>*Med. Phys. Lab., Dept of Medicine, University of Ioannina, 45110, Ioannina, Greece*

<sup>f</sup>*Université de Bordeaux, CNRS, LP2I Bordeaux, UMR 5797, Chemin du*

*Solarium, 19, 33170, Gradignan, France*

<sup>g</sup>*ISMN-CNR, p. Aldo Moro, 7, 00185, Rome, Italy*

---

## Abstract

Cosmic rays have the potential to significantly affect the atmospheric composition by increasing the rate and changing the types of chemical reactions through ion production. The amount and states of ionization, and the spatial distribution of ions produced are still open questions for atmospheric models. To precisely estimate these quantities, it is necessary to simulate particle–molecule interactions, down to very low energies. Models enabling such simulations require interaction probabilities over a broad energy range and for all energetically allowed scattering processes.

In this paper, we focus on electron interaction with the two most abundant molecules in the atmosphere, i.e., N<sub>2</sub> and O<sub>2</sub>, as an initial step. A set of elastic and inelastic cross section models for electron transportation in oxygen and nitrogen molecules valid in the energy range 10 eV - 1 MeV, is presented. Comparison is made with available theoretical and experimental data and a reasonable good agreement is observed. Stopping power is calculated and compared with published data to assess the general consistency and reliability of our results. Good overall agreement is observed, with relative differences lower than 6% with the ESTAR database.

*Keywords:* Electron cross sections, Atmosphere ionization, Particle track structure, Monte Carlo simulation, Geant4-DNA

---

## 1. Introduction

The emission of polluting molecules and greenhouse gases into the atmosphere represents a global challenge with open scientific questions, mainly related to the approximation grade of chemical-physical processes used in the prevision models of climate change. Although ions play a pivotal role in various atmospheric processes such as ion-induced nucleation, precipitation, and aerosol formation, the influence of

---

\*Correspondence: francesca.nicolanti@uniroma1.it

13 cosmic rays and ions on climate is at the dawn of a full understanding and deserves  
14 further in-depth investigations [1].

15 Chemical reaction rates can vary by up to 10 orders of magnitude depending on  
16 the ionization state of the involved species [2, 3]. Thus, cosmic rays ionization could  
17 significantly impact chemical reactions in the atmosphere, considering also that the  
18 ions produced are clustered near the primary ray. The amount and state of ionization,  
19 as well as the spatial distribution of ions in the atmosphere, are open questions for the  
20 atmospheric models, that it is fundamental to investigate also in the very low-energy  
21 range [4, 5, 6].

22 Oxygen and nitrogen molecules are the two most prevalent species in Earth’s tro-  
23 posphere and lower stratosphere. Therefore, studying the interaction of cosmic rays  
24 with these molecules is crucial for our understanding of various atmospheric phe-  
25 nomena. For instance, electron impact ionization plays a role in the inter-conversion  
26 between ozone and oxygen in the atmosphere, while nitrogen is involved in the pro-  
27 duction of one of the most dangerous greenhouse gasses: nitrous oxide [7, 8, 9]. The  
28 ejection of secondary electrons in collisions with individual molecules represents the  
29 elementary process involving the greatest energy transfer and is of central interest  
30 in any study concerning the interaction of charged particles with matter. For large  
31 energy ranges, it is also the most likely process.

32 Event-by-event simulations are a powerful tool for studying the details of radiation-  
33 induced effect at the molecular level. Nowadays, several existing Monte Carlo track-  
34 structure (MC-TS) codes fulfill this purpose. One of these is Geant4-DNA [10, 11, 12,  
35 13], an extension of Geant4 (GEometry ANd Tracking) [14, 15, 16] which is the most  
36 widely used toolkit for performing MC simulations of radiation-matter interactions.  
37 Geant4-DNA makes it possible to explicitly simulate every single electromagnetic par-  
38 ticle interaction down to low energy (about 10 eV), as well as diffusion and chemical  
39 reactions, on some specific materials of interest in radiobiology [17, 18].

40 The aim of this work is to provide a comprehensive and reliable set of electron  
41 impact electromagnetic interaction models for O<sub>2</sub> and N<sub>2</sub> molecules down to the 10  
42 eV scale, for use in such simulation code. This will allow to accurately simulate the  
43 interaction of low-energy secondary radiation with molecules, the exact concentration  
44 of ions produced, their spatial distribution, and the ionization state.

45 We selected a model for each relevant electromagnetic electron impact interaction  
46 process in the energy range 10eV - 1MeV, including ionization, electronic excitation,  
47 and elastic scattering. Given the computational constraints of a simulation code,  
48 we focused on choosing calculation methods that are both sustainable and efficient.  
49 In this regard, models that provide an analytical expression for the cross section  
50 and a good compromise between accuracy and computational time were preferred.  
51 The physics models presented here can be easily adapted to be used for molecules  
52 in the gas phase and further work is planned to extend them to other species of  
53 climate interest. One of these is the trace gas SO<sub>2</sub>, studied at CERN in the CLOUD  
54 experiment [19, 20], which has proven to have large effects on ozone chemistry.

55 The selected models are briefly described in Sec. 2. In Section 3, we present  
56 the benchmark of our models implementation. Specifically, in section 3.1, we show  
57 the partial cross sections obtained for each process and compare them with exper-  
58 imental data or other calculations. In section 3.2, we provide a final validation by  
59 comparing the calculated stopping power, obtained using the selected models, with  
60 semi-empirical results and ab-initio calculations. The stopping power is also compared  
61 with the ICRU (International Commission on Radiation Units and Measurements)  
62 recommended values calculated by ESTAR available down to 1 keV, which are a good  
63 benchmark for MC calculations. The ESTAR values have uncertainties ranging from  
64 1% to 2% (in low-Z materials), for energies higher than 10 keV. These uncertainties  
65 grow up to 10% at 1keV, due to the omission of shell corrections [21].

## 66 2. Description of physics models

### 67 2.1. Ionization

68 Electron impact ionization is based on the Relativistic Binary Encounter Bethe  
69 (RBEB) model [22], which combines the relativistic Mott cross section, known as  
70 the Møller cross section, with the relativistic version of the Bethe cross section. It  
71 represents the high-energy extension of the corresponding Binary Encounter Bethe  
72 model developed by Kim and Rudd [23].

73 Within the framework of this model, the energy differential cross section (DCS)  
74  $\frac{d\sigma_{MO}(t)}{dw}$  with the energy of the ejected electron  $W$  at a given incident energy  $T$  for a  
75 molecular orbital ( $MO$ ), can be written as

$$\begin{aligned} \frac{d\sigma_{MO}}{dw} = & \frac{4\pi a_0^2 \alpha^4 N}{(\beta_t^2 + \beta_u^2 + \beta_b^2) 2b'} \left[ -\frac{1}{t+1} \left( \frac{1}{w+1} + \frac{1}{t-w} \right) \times \frac{1+2t'}{(1+t'/2)^2} \right. \\ & + \frac{1}{(w+1)^2} + \frac{1}{(t-w)^2} + \frac{b'}{(1+t'/2)^2} + \left( \ln \left( \frac{\beta_t^2}{1-\beta_t^2} \right) - \beta_t^2 - \ln(2b') \right) \\ & \left. \times \left( \frac{1}{(w+1)^3} + \frac{1}{(t-w)^3} \right) \right] \quad (1) \end{aligned}$$

where

$$t = T/B, \quad w = W/B, \quad u = U/B$$

$$\beta_t^2 = 1 - \frac{1}{(1+t')^2}, \quad t' = T/m_e c^2$$

$$\beta_u^2 = 1 - \frac{1}{(1+u')^2}, \quad u' = U/m_e c^2$$

$$\beta_b^2 = 1 - \frac{1}{(1+b')^2}, \quad b' = B/m_e c^2$$

76 The RBEB formula depends only on the three input parameters, i.e. the binding  
 77 energy ( $B$ ), the mean kinetic energy ( $U$ ) and the occupancy number ( $N$ ) of each  
 78 molecular orbital. The simple analytical form in Eq. 1 is ideally suited for modeling  
 79 applications and Monte Carlo simulation as it allows energy loss to be randomly  
 80 sampled during an ionization event without the need for lengthy cross sections tables  
 81 [24].

82 This model is valid for electron energies that are significantly higher than the  
 83 binding energy of the target electron, as it is based on the First Born Approximation.  
 84 Nevertheless, for many stable molecules including  $N_2$  and  $O_2$ , it yields ionization cross  
 85 sections that are in good agreement in both magnitude (with deviations of 15% or  
 86 less at the peak) and shape from each shell ionization threshold onwards [25, 26]. We  
 87 have imposed the high-energy limit to 1 MeV, as for higher energies other relativistic  
 88 effects, such as the density effect, must be considered.

89 In the RBEB model the scattering angle of the primary electron and the ejected  
 90 angle of the secondary electron are assumed to be isotropic. This approximation can  
 91 be reduced by introducing a sampling of both angles determined by the kinematics  
 92 of binary collisions [28].

93 The ionization cross section for each molecular orbital is given by integration of  
 94 Eq. 1 up to the maximum energy of the ejected electron  $W_{max} = (T - B)/2$ , namely,

$$\begin{aligned} \sigma_{MO}^{Ioni} = & \frac{4\pi a_0^2 \alpha^4 N}{(\beta_t^2 + \beta_u^2 + \beta_b^2) 2b'} \times \left\{ \frac{1}{2} \left[ \ln \left( \frac{\beta_t^2}{1 - \beta_t^2} \right) - \beta_t^2 - \ln(2b') \right] \times \left( 1 - \frac{1}{t^2} \right) \right. \\ & \left. + 1 - \frac{1}{t} - \frac{\ln t}{t+1} \frac{1+2t'}{(1+t'/2)} + \frac{b'^2}{(1+t'/2)^2} \frac{t'-1}{2} \right\} \end{aligned} \quad (2)$$

95 For single ionization of inner k-shells which are subject to stronger nuclear attrac-  
 96 tion, we use the averaged RBEB formula [22, 27]:

$$\sigma_{k-shell}^{Ioni} = \frac{1}{2} \left( 1 + \frac{\beta_t^2 + \beta_u^2 + \beta_b^2}{\beta_t^2} \right) \times \sigma_{MO}^{Ioni} \quad (3)$$

97 For oxygen molecules there are five outer shells and the inner K-shell of the oxygen  
 98 atom, while for nitrogen molecules there are four outer shells plus the inner K-shell  
 99 of the nitrogen atom. For each outer shell, the binding energies and the mean kinetic  
 100 energies are from Hwang et al. [29], while K-shells parameters for diatomic molecules  
 101 are from Jolly et al [30] (Table 1).

## 102 2.2. Elastic scattering

103 Elastic scattering, although involving only minimal energy loss, strongly influences  
 104 the accuracy of the spatial distribution of energy deposition.

105 To calculate the differential and integral elastic cross sections we used the IAM-  
 106 SCAR method, which is based on the Independent Atom Model representation (IAM)[31]

Table 1: Required set of parameters for the calculation of ionization cross sections in molecular nitrogen and oxygen with the RBEB model.

		Ionization		
	Molecular Orbital	Threshold B (eV)	Mean kinetic energy U (eV)	N
N <sub>2</sub>	2σ <sub>g</sub>	41.72	71.13	2
	2σ <sub>u</sub>	21.00	63.18	2
	1π <sub>u</sub>	17.07	44.30	4
	3σ <sub>g</sub>	15.58	54.91	2
	k-shell	409.5	603.3	4
O <sub>2</sub>	2σ <sub>g</sub>	46.19	79.73	2
	2σ <sub>u</sub>	29.82	90.92	2
	1π <sub>u</sub>	19.64	59.89	4
	3σ <sub>g</sub>	19.79	71.84	2
	1π <sub>g</sub>	12.07	84.88	2
	k-shell	543.8	796.2	4

107 complemented with a Screening-Corrected Additivity Rule (SCAR) [32, 33]. This  
 108 method has already been extensively employed to calculate electron-scattering cross  
 109 sections for a wide variety of molecular targets, over a broad energy range [34, 35, 36,  
 110 37, 38].

111 Under the IAM approximation, the scattering from a molecule is described by the  
 112 direct and spin-flip scattering amplitudes:

$$F(\theta) \approx \sum f_i(\theta)e^{i\mathbf{q}\cdot\mathbf{r}_i} \quad \text{and} \quad G(\theta) \approx \sum g_i(\theta)e^{i\mathbf{q}\cdot\mathbf{r}_i} \quad (4)$$

113 where  $q = k_f - k_i$  is the momentum transfer,  $r_i$  are the atomic positions, and  $f_i(\theta)$   
 114 and  $g_i(\theta)$  are the atomic scattering amplitudes. By averaging the modulus squared  
 115 of the scattering amplitudes  $|F(\theta)|^2$  and  $|G(\theta)|^2$  over all molecule orientations [2,6],  
 116 we obtain the differential elastic cross section:

$$\begin{aligned} \frac{d\sigma_{molecule}^{elastic}}{d\Omega} &= \sum_{i,j} [f_i(\theta)f_j^*(\theta) + g_i(\theta)g_j^*(\theta)] \frac{\sin(qr_{ij})}{qr_{ij}} = \sum_i [|f_i(\theta)|^2 + |g_i(\theta)|^2] + \\ &\sum_{i \neq j} [f_i(\theta)f_j^*(\theta) + g_i(\theta)g_j^*(\theta)] \frac{\sin(qr_{ij})}{qr_{ij}} = \sum_i \frac{d\sigma_{atom}^{elastic}}{d\Omega} + \frac{d\sigma^{interference}}{d\Omega} \end{aligned} \quad (5)$$

117 where  $q \equiv |\mathbf{q}| = 2k \sin(\theta/2)$  and  $r_{ij}$  is the distance between the  $i$  and  $j$  atoms. By  
 118 integrating Eq. (5), the total molecular cross section can be written as:

$$\sigma_{molecule}^{IAM} = \sum_i \sigma_i + \sigma^{interference} = \sigma^{AR} + \sigma^{interference} \quad (6)$$

119 The first term  $\sigma^{AR}$  corresponds to the direct sum of atomic cross sections and it

120 is equivalent to the molecular cross sections according to the Additivity Rule (AR)  
 121 [39]. The second term  $\sigma^{interference}$  represents the interference contribution between  
 122 two single scattering events. Its main effect is to increase the differential cross sections  
 123 at small scattering angles ( $\theta < 30^\circ$ ), leading to an overall increase in the integral cross  
 124 section values. It must be noted that the second contribution would not be present in  
 125 Eq. (6) if this expression were directly obtained from Eq. (4) by applying the optical  
 126 theorem. Thus, differential cross sections should be renormalized to avoid inherent  
 127 contradictions [35, 36].

128 The above expressions are applicable for independent scattering from each atom  
 129 and they are only valid for large interatomic distances compared to the wavelength  
 130 associated with the incident electron ( $\sim < 200$  eV for  $N_2$  and  $O_2$ ). To extend their  
 131 applicability to lower energies, the SCAR method introduces screening coefficients  
 132 ( $s_i$ ) in Eq. 5-6. These coefficients have the effect to reduce the contribution of each  
 133 atom to the overall molecular cross section ( $0 \leq s_i \leq 1$ ) in the low energy range.  
 134 Further details on these coefficients can be found elsewhere [32, 33, 40].

135 Atomic scattering amplitudes and cross sections in Eq. (5) were calculated us-  
 136 ing the ELSEPA (ELastic Scattering of Electrons and Positrons by neutral Atoms)  
 137 code developed by Salvat et al. [41], which uses the Dirac partial-wave approach  
 138 including relativistic corrections to calculate the electron elastic scattering by a local  
 139 central interaction potential representing atoms. To perform the calculation in the  
 140 optical potential formalism, we considered the Fermi nucleus distribution, the Dirac-  
 141 Fock electron distribution, the Furness-McCarthy exchange potential, the correlation-  
 142 polarization potential with the local density approximation, and the LDA absorption  
 143 potential, described in detail in Ref. [41].

144 In our study, we observed that including the interference terms gives good agree-  
 145 ment with reference data at small scattering angles ( $< 30^\circ$ ), but results in a significant  
 146 overestimation of integral cross sections (as shown later in Fig. 5). Consequently, we  
 147 decided to employ the simple incoherent sum of atomic scattering amplitudes, follow-  
 148 ing the AR approximation. This approach not only eliminates the need for renormal-  
 149 ization to satisfy the optical theorem, but also significantly enhances the agreement  
 150 between the total cross sections (TCSs) and the experimental data, as previously  
 151 stated in [42].

152 Nevertheless, to enhance the accuracy of our calculations, we introduced slight  
 153 adjustments to the free parameters of the scattering potential, specifically target-  
 154 ing an increase in the differential cross sections at small scattering angles. The two  
 155 parameters involved are  $b_{pol}$  and  $A_{abs}$ , included in the correlation polarization poten-  
 156 tial and the absorption potential, respectively. The default values used in ELSEPA  
 157 have been validated for noble gases and mercury, but they can be modified to better  
 158 match experimental data. Notably, above the ionization threshold, a higher absorp-  
 159 tion strength increases the DCSs at small scattering angles while decreasing them at  
 160 intermediate and large angles. As for the  $b_{pol}$  parameter, the DCSs at small angles  
 161 are the highest when  $b_{pol}$  is the lowest and decrease with increasing  $b_{pol}$ .

162 By examining the impact of these two parameters on the DCS, we qualitative  
 163 determined optimized values for  $b_{pol}$  and  $A_{abs}$ . Specifically, for energies below 500 eV,  
 164 the value of  $b_{pol}$  is fixed at 0.01. As the energy approaches 1 keV, it linearly increases  
 165 from 0.01 to 6.6. Beyond 1 keV, the expression  $\sqrt{\frac{E(eV)-50eV}{22eV}}$  governs the behavior of  
 166  $b_{pol}$  for both molecules. Regarding the  $A_{abs}$  parameters for  $N_2$ , it decreased linearly  
 167 from 2.5 at 12 eV to 2 at 400 eV. For  $O_2$ ,  $A_{Abs}$  transitions from 2 at 12 eV to 3 at 70  
 168 eV, and then decreases back to 2 at 300 eV. For higher energies,  $A_{Abs}$  is set to 2 for  
 169 both molecules, which corresponds to the default value proposed by ELSEPA.

170 It should be made clear that the cross sections for each constituent atom are  
 171 calculated using the known first optically allowed excitation threshold [88] and atomic  
 172 polarizability [44] of that atom, prior to the application of the screening corrected  
 173 additivity rule. The bond distances are taken from the pubchem database of 3D  
 174 molecular structures [38]. For  $N_2$ , the bond length is  $1.12\text{\AA}$ , while for  $O_2$ , it is  $1.23\text{\AA}$   
 175 [43].

### 176 2.3. Electronic excitation

177 The third process which is of great importance during electron slowing down in  
 178 the atmosphere is the excitation of molecules by electron impact. This process plays  
 179 an important role in determining the internal energy and state distribution of the  
 180 gaseous molecules in the atmosphere, and is mainly responsible for the increase of the  
 181 mean energy loss in the low energy region.

182 The treatment of excitation process in oxygen and nitrogen is based on the rela-  
 183 tivistic formulae of Porter et al. [47]. For optically forbidden discrete excitations the  
 184 cross section  $\sigma_j^{exc}$  to a state  $j$  of electrons at energy  $T$  is given by :

$$\sigma_j^{exc,forbidden} = \frac{q_0 A \phi (2W_j/m\beta^2 c^2)}{(m\beta^2 c^2/2W_j) W_j^2} \quad (7)$$

where

$$\phi (2W_j/m\beta^2 c^2) = \frac{[1 - (2W_j/m\beta^2 c^2)^\alpha]^\beta}{(m\beta^2 c^2/2W_j)^{\Omega-1}}$$

185 is a distortion factor and allows for variations from the asymptotic Bethe formula  
 186 at low energies.  $q_0 = 4\pi a_0^2 R^2$  and has the numerical value of  $6.513 * 10^{-14} eV^2 cm^2$ ,  
 187  $a_0$  being the Bohr radius and  $R$  the Rydberg energy.  $W_j$  is the threshold excitation  
 188 energy of the  $j^{th}$  states, and  $A$ ,  $\alpha$ ,  $\beta$  and  $\Omega$  are four adjustable parameters.

189 The second form used to represent the cross section of discrete allowed excitations  
 190 and for the excitation of Rydberg states is more consistent with the asymptotic form  
 191 of Born-Bethe theory, and is calculated according to:

$$\sigma_j^{exc,allowed} = \frac{q_0 A \phi (2W_j/m\beta^2 c^2)}{(m\beta^2 c^2/2W_j) W_j^2} \left\{ \ln \left[ 4 \left( \frac{m\beta^2 c^2}{2W_j} \right) \frac{C_j}{(1 - \beta^2)} + e \right] - \beta^2 \right\} \quad (8)$$

where  $\phi(2W_j/m\beta^2c^2)$  is given by

$$\phi(2W_j/m\beta^2c^2) = \left[1 - \left(\frac{2W_j}{m\beta^2c^2}\right)^\alpha\right]^\beta \Theta\left(\frac{m\beta^2c^2}{2W_j} - 1\right)$$

192 with

$$\Theta\left(\frac{m\beta^2c^2}{2W_j} - 1\right) = \begin{cases} 1, & m\beta^2c^2/2 \geq W_j \\ 0, & m\beta^2c^2/2 < W_j \end{cases} \quad (9)$$

193 We determined the free parameters in Eq. 7-8 ( $A$ ,  $\alpha$ ,  $\beta$  and  $\Omega$ ) for most of the  
 194 excitation states through a non-linear least squares analysis of various experimental  
 195 data sets, following the procedure outlined in [48]. In cases where literature data  
 196 were unavailable, the values for the excitation parameters were taken from the study  
 197 by Porter et al [47]. The cross section parameters and formulas for the excitation of  
 198 Rydberg states were also taken from the publication by Porter et al. Their formulas  
 199 employ a method to calculate the  $A$  and  $W_j$  parameters for each Rydberg series, that  
 200 takes into account the principal quantum number and the quantum defect associated  
 201 with the specific state.

Table 2: Excitation cross section parameters for use in formulas 7-8. Those marked with (\*) are from Porter et al [47], while the remaining parameters are obtained through fitting data or other models, as described in the text. Excitation threshold energies come from Itikawa, and Porter et al. [45, 46, 47].

		Excitation				
State	$W_j(eV)$	$A$	$\Omega$	$\gamma$	$\nu$	
vib $\nu$ 1-3 (*)	1.85	0.273	7	1	1	
vib $\nu$ 4-8 (*)	2.15	0.241	9	1	1	
$A^3\Sigma_u^+$	6.169	0.04	1.51	7.37	12.12	
$B^3\Pi_g$	7.353	0.06	1.71	9.0	7.0	
$W^3\Delta_u$	7.362	0.08	1.77	5.63	11.5	
$B'^3\Sigma_u^-$	8.165	0.04	1.69	16.7	714	
$a^1\Sigma_u^-$	8.399	0.01	1.56	15.0	13.1	
$N_2$ $a^1\Pi_g$	8.549	0.09	1.00	7.93	9.56	
$w^1\Delta_u$	8.89	0.01	1.05	16.4	9.6	
$C^3\Pi_u$	11.032	1.17	2.25	0.07	0.57	
$E^3\Sigma_g^+$ (*)	11.875	0.048	3.00	3.00	1.	
$a'^1\Sigma_g^+$	12.255	0.15	1.59	0.32	0.9	
$b^1\Pi_u$	12.5	0.12	0.85	1.29	2.34	
$b^1\Sigma_u^+$	13.3	0.25	0.06	1.03	2.63	
$c_4^1\Sigma^+$	12.94	0.23	0.05	-1.1	4.05	
$a_1\Delta_g$	0.98	0.11	2.23	0.7	9	
$b_1\Sigma_g^+$	1.63	0.008	2.01	1	6	
$A^3\Sigma_u^+$ (*)	4.5	0.02	0.9	1	1	
$O_2$ $2B$	10.29	0.008	0.17	0.8	1.3	
$LB$	9.96	0.009	0.93	1.5	0.4	
$B^3\Sigma_u^-$	6.12	0.13	0.21	1.7	2	

202 The excitation of three possible allowed states ( $B^3\Sigma_u^-$ , Longest Band-LB, Second

203 Band-2B), three forbidden states ( $b^1\Sigma_g^+$ ,  $a^1\Delta_g$ ,  $A^3\Sigma_u^+$ ), plus 21 Rydberg states (7 with  
 204 principal quantum number equal to 3, 7 with principal quantum number equal to 4,  
 205 and 7 cumulative for all higher lying members), was taken into account in the present  
 206 study for oxygen.

207 For molecular nitrogen three allowed levels ( $b^1\Pi_u$ ,  $b^1\Sigma_u^+$ ,  $c_4^1\Sigma^+$ ), twelve forbidden  
 208 levels (vib  $\nu$  1-3, vib  $\nu$  4-8,  $A^3\Sigma_u^+$ ,  $B^3\pi_g$ ,  $W^3\Delta_u$ ,  $B'^3\Sigma_u^-$ ,  $a'^1\Sigma_u^-$ ,  $w^1\Delta_u$ ,  $C^3\Pi_u$ ,  $E^3\Sigma_g^+$ ,  
 209  $a^1\Pi_g$ ,  $a''^1\Sigma_g^+$ ), plus 18 Rydberg states (6 with principal quantum number equal to 3,  
 210 6 with principal quantum number equal to 4, and 6 cumulative for all higher lying  
 211 members), have been included. The values of the forbidden and allowed excitation  
 212 parameters used in the present study and partially based on Porter et al. are listed in  
 213 table 2. For the parameters related to the excitation of Rydberg states, please refer  
 214 to [47].

215 For the use of such a model for simulation purposes, the excitation of Rydberg-  
 216 like states that often leads to auto-ionization needs to be considered. Following  
 217 the recommendations of Stolarski [49] and Watson [50], a 50% probability of auto-  
 218 ionization should be assumed when the excitation energy of a Rydberg state is greater  
 219 than the ionization threshold for the material.

### 220 3. Results and discussion

221 We implemented the described models in C++, with the aim of interfacing them  
 222 with Geant4-DNA in the near future. The computation of ionization and excita-  
 223 tion cross sections is performed using their analytical formulations. As for elastic  
 224 cross sections, we have employed interpolated cross section data tables, following the  
 225 approach commonly used in particle transport codes.

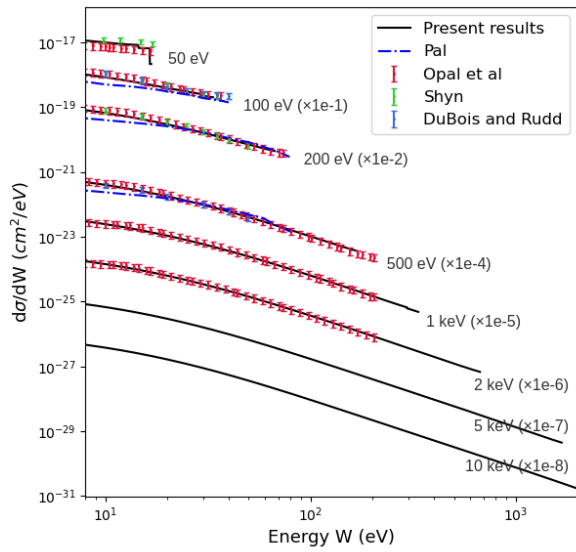
#### 226 3.1. Cross sections

##### 227 3.1.1. Differential Ionization Cross Section

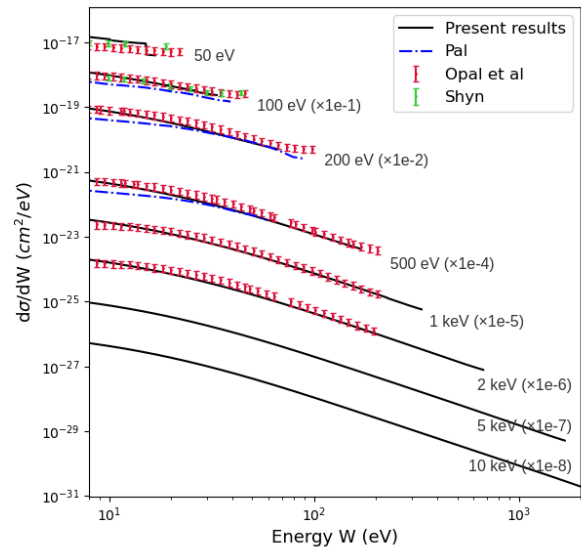
228 For a given incident energy, the sum of Eq. 2 over all molecular orbitals gives  
 229 the energy differential ionization cross-section. This has been evaluated at impinging  
 230 electron energies varying from 10 eV to 1 MeV employing the RBEB formulation. In  
 231 Fig. 1, the results are compared with the experimental cross sections from Opal et al  
 232 [51], Shyn [52, 53], DuBois and Rudd [54], and the theoretical data from Pal et al [55],  
 233 computed by using the the Jain-Khare semiempirical approach [56]. The differential  
 234 cross sections reveal a good agreement with the experimental values and better than  
 235 those determined from the Jain-Khare method. The main differences are observed  
 236 for an incident electron energy of 50 eV, for which there is also strong disagreement  
 237 between Shyn's and Opal's experimental data (about 50%).

##### 238 3.1.2. Differential Elastic Cross Sections

239 The elastic DCSs for electron scattering by N<sub>2</sub> and O<sub>2</sub>, obtained using the SCAR  
 240 model with the proposed expression for  $b_{pol}$  and  $A_{abs}$ , are presented in Figures 2-3.



(a) N<sub>2</sub>



(b) O<sub>2</sub>

Figure 1: Differential cross sections for ionization by electrons in molecular nitrogen (a) and oxygen (b) as a function of the ejected electron energy  $W$ , for several incident electron energies from the RBEB model (solid black lines). To improve the readability of the plot, the DCS results are presented only in the energy range of 50 eV to 10 keV (no experimental data are available in the literature for energies higher than 2 keV). Experimental data from Opal et al. [51], Shyn and Sharp [52], Shyn [53], and Du Bois and Rudd [54] are shown in symbols with their uncertainties; the semi-empirical data from Pal et al. [55] are shown in dash-dot blue line.

241 These results are compared with the ones obtained using the AR model, employing  
242 the default expression parameters from ELSEPA, as well as experimental data.

243 It is observed that the SCAR corrections lead to a decrease in the DCSs across  
244 the entire scattering angle range and particularly for energies below 200 eV, for both  
245 molecules. This correction significantly improves the agreement between the calcu-  
246 lated DCSs and the experimental data, even at energies as low as 15 eV. The modified  
247 potential parameters increase the DCSs at zero angles by 4 % to 34% for energies  
248 higher than about 50 eV, while improving the overall shape of the DCSs at energies  
249 below 300eV. At high energies, our elastic model yields good results in reasonable  
250 agreement with the experimental data. In the case of oxygen, a slight underestimation  
251 of the DCSs at angles lower than 20° is observed when compared to the experimental  
252 data from Iga et al. [69], and Daimon et al. [71]. This discrepancy becomes more  
253 pronounced in the energy range of 100-500 eV. However, these results are reflected in  
254 higher TCS compared to other experimental findings, as will be discussed later.

### 255 3.1.3. Excitation Cross Sections

256 In Fig. 4 the excitation cross sections for each of the levels included in the present  
257 study are shown, along with experimental or semi-empirical data used for the fitting  
258 procedure. The cross sections trend at low energies and for the lower states is mainly  
259 based on the values recommended by Itikawa [45, 46]. In the absence of experimental  
260 data in the intermediate-high energy range, the asymptotic dependence was obtained  
261 through data transcribed from S.F. Biagi’s FORTRAN code (MagBoltz, versions 8.9  
262 and later) [72, 73] and the semi-empirical BEF-scaling results [77, 78, 80] for the  
263 dipole-allowed transitions.

### 264 3.1.4. Total Cross Sections

265 The total scattering cross section  $\sigma^{tot}$  of electrons at energy  $T$  in nitrogen and  
266 oxygen was calculated as  $\sigma^{tot} = \sigma^{ion} + \sigma^{el} + \sigma^{exc}$  and can be compared in Fig. 5 with  
267 the recommended values by Itikawa and other cross section results. The individual  
268 contributions of ionization, excitation, and elastic processes are presented in solid  
269 lines, alongside experimental data and semi-empirical calculations (further details in  
270 the plot legend).

271 As expected, the excitation  $\sigma_{exc}$  and ionization  $\sigma_{ion}$  cross sections exhibit similar  
272 energy dependence for energies above approximately 200 eV, but  $\sigma_{exc}$  increases with  
273 decreasing energy due to the contribution of excitation to optically forbidden states.  
274 A glance at the figures shows that the high values of the elastic cross section, compared  
275 to those of other interaction effects, are remarkable at energies smaller than 100 eV.

276 The elastic cross section results demonstrate good agreement with all experimental  
277 data sets for N<sub>2</sub>. For oxygen, small deviations are noticed for energies below 60  
278 eV [45, 86]. Nevertheless, these deviations are still within the range of Itakawa’s  
279 experimental uncertainties ( $\pm 20\%$ , not displayed in the plot).

280 The results obtained from the IAM-SCAR model are included for comparison in  
281 Fig. 5. As previously mentioned, the inclusion of the interference term in Eq. (6)

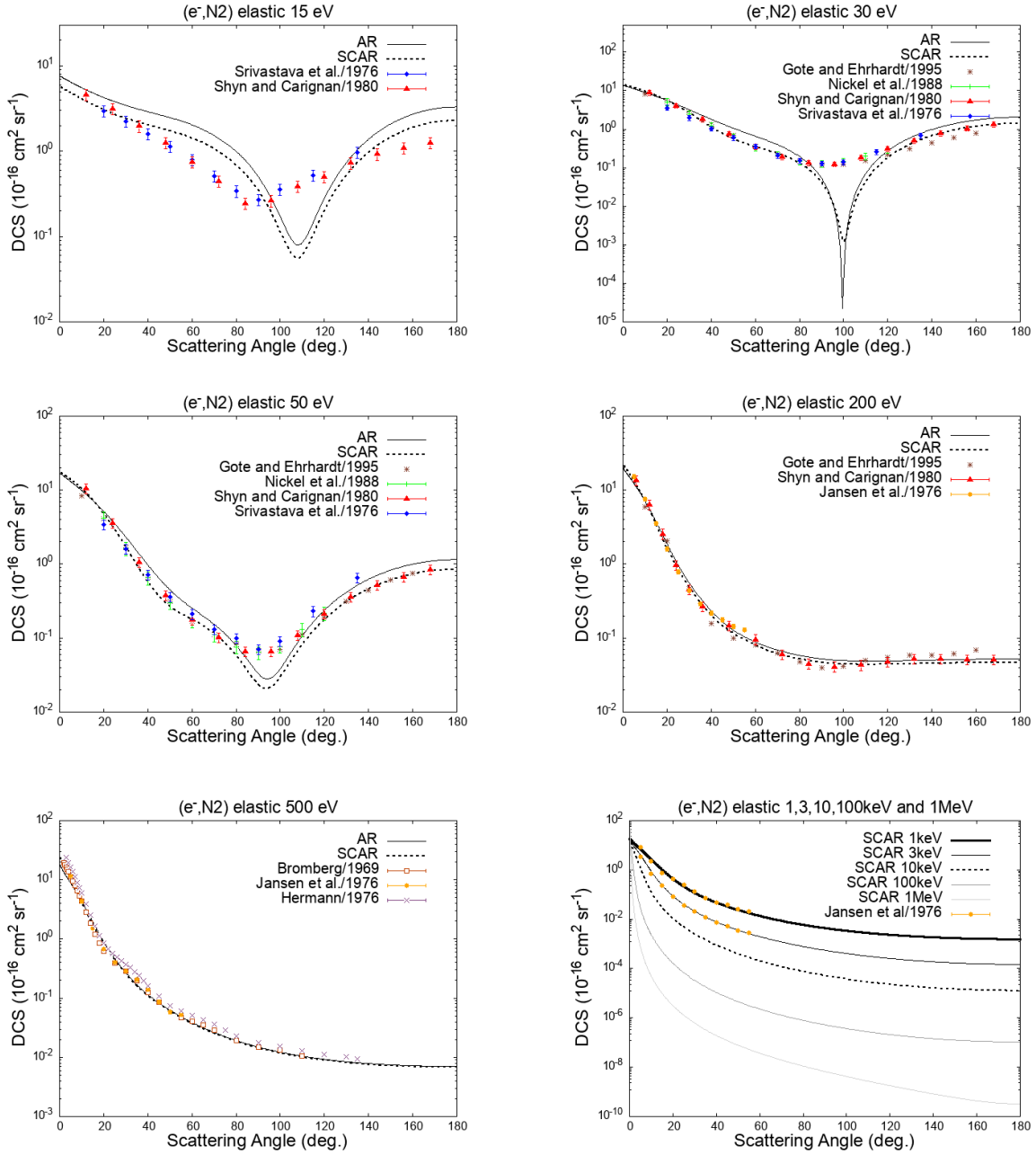


Figure 2: Differential cross sections for the elastic scattering of electrons from nitrogen at energies 15, 30, 50, 200 eV; 0.5, 1, 3, 10, 100 keV and 1 MeV, obtained by applying the AR and SCAR models to the atomic results from the ELSEPA code. Experimental data are from: Gote and Ehrhardt [57], Shyn and Carignan [58], Srivastava et al. [59], Nickel et al. [60], Jansen et al. [61], Herrmann [62] and Bromberg [63].

282 leads to an overall increase in the integral elastic cross section across the entire energy  
 283 range. Specifically, this enhancement is about 26% and 24% at 100 eV for N<sub>2</sub> and

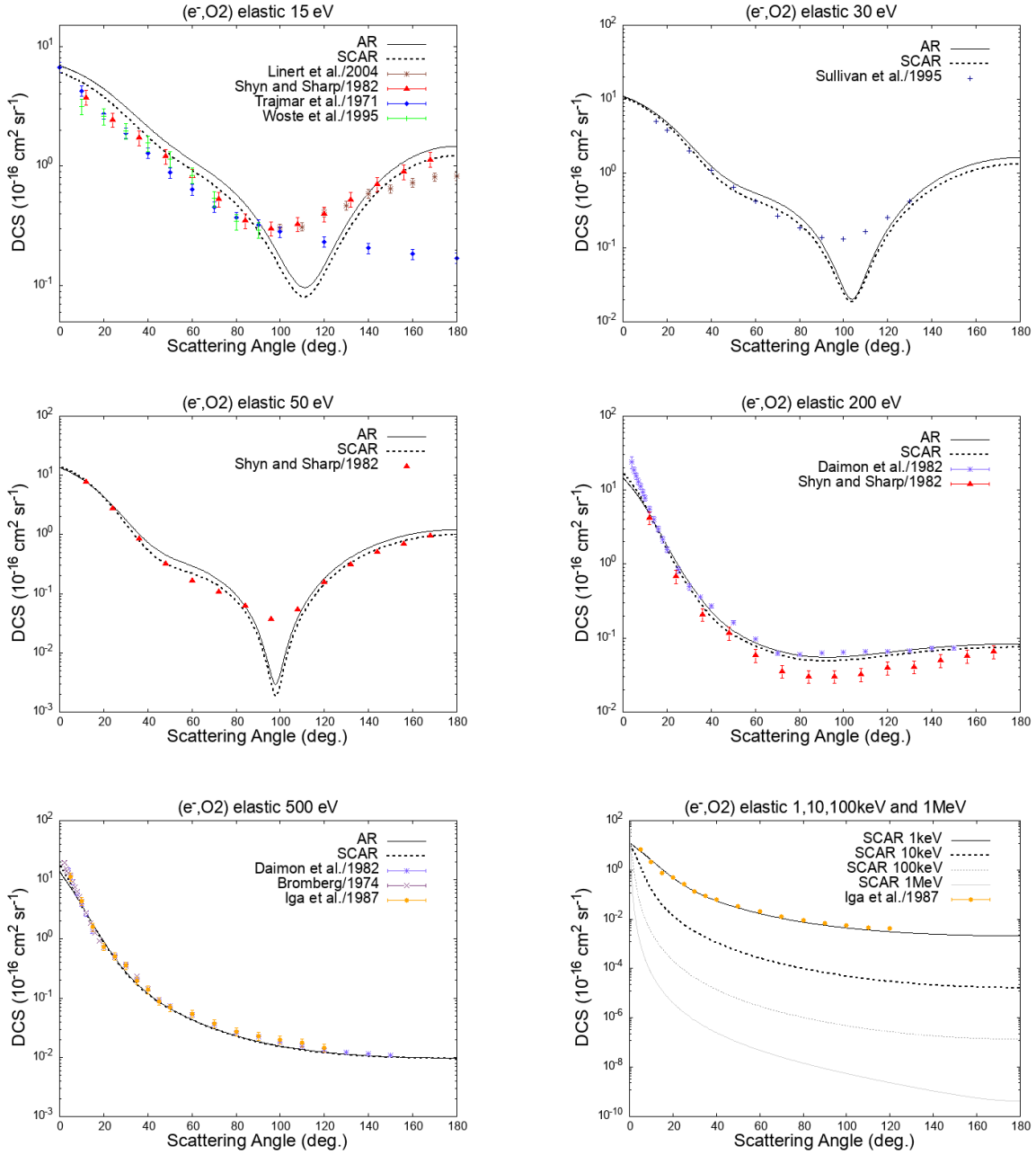


Figure 3: Differential cross sections for the elastic scattering of electrons from oxygen at energies 15, 30, 50, 200 eV; 0.5, 1, 10, 100 keV and 1 MeV, obtained by applying the AR and SCAR models to the atomic results from the ELSEPA code. Experimental data are from: Linert et al. [64], Shyn and Sharp [65], Trajmar et al. [66], Woste et al. [67], Sullivan et al. [68], Iga et al. [69], Bromberg [70], and Daimon et. al.[71].

284 O<sub>2</sub>, respectively, and decreases to 15% and 10% at 10 keV. It is worth noting that the  
 285 experimental values from Iga et al. [69], and Daimon et. al [71] for O<sub>2</sub> demonstrate  
 286 better agreement with the IAM-SCAR model compared to the AR-SCAR approxi-

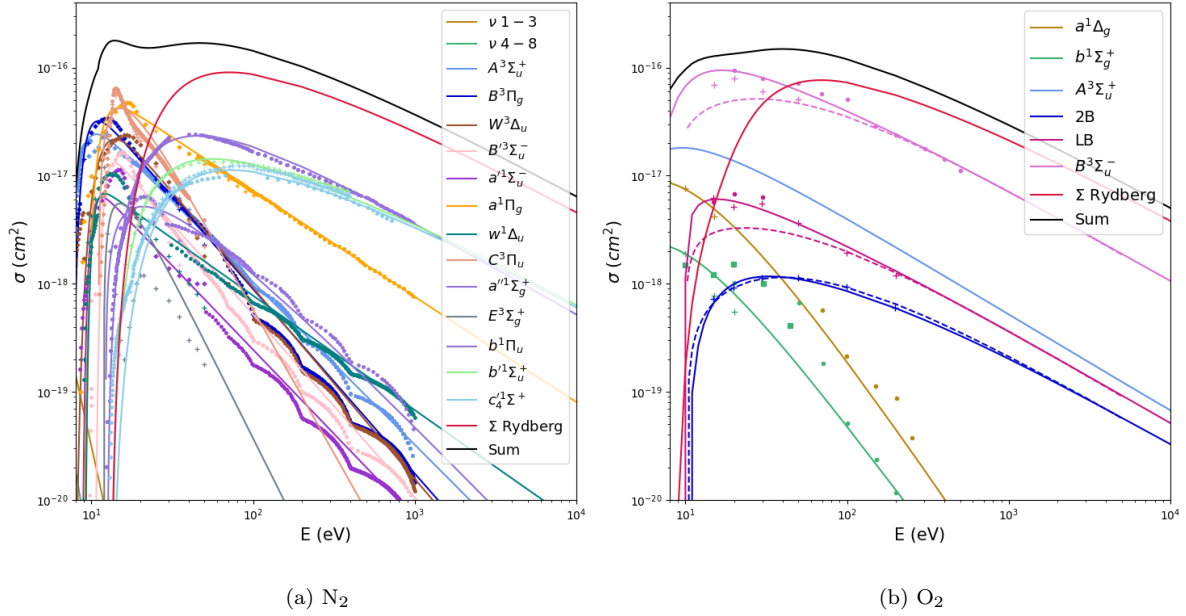


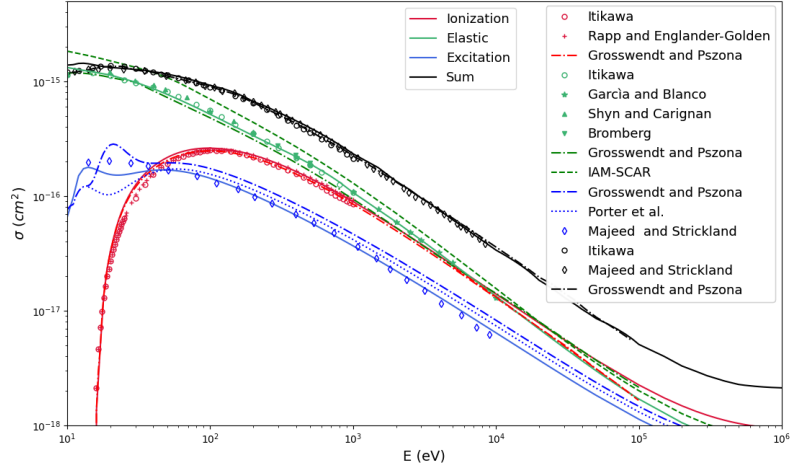
Figure 4: Excitation cross sections for nitrogen (a) and oxygen (b) molecules obtained from Porter's formula with the parameters given in Table 2. To improve the readability of the plot, the DCS results are presented only in the energy range of 10 eV to 10 keV. The excitation cross sections for nitrogen are compared with experimental values from Itikawa (crosses) [46] and data from S.F. Biagi (dots) [72, 73]. The excitation cross sections for oxygen are compared with experimental data from Itikawa (crosses) [45], Wakiya (dots) [74], Trajmar et al. (squares) [75], Linder and Schmidt (asterisks) [76] and semi-empirical BEf-scaling (dashed lines) results from [78]. The sums over all the Rydberg states for both molecules are also shown.

287 mation. This overestimation of the TCS when compared to more recent experimental  
288 data is also reflected in their small-angle DCSs in Figure 3, that show higher values  
289 in comparison to the predictions of the AR-SCAR model.

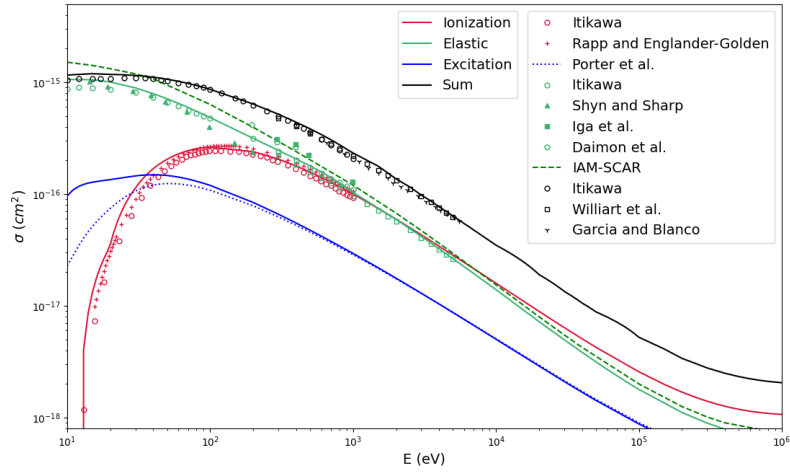
290 In Fig. 5 the excitation cross sections obtained in the present study are com-  
291 pared with those obtained using Porter’s default parameters. For oxygen, the fitting  
292 procedure based on the most recent cross section measurements allows for a better  
293 description of the cross section at very low energies, while maintaining the same be-  
294 havior at intermediate and high energies. As for nitrogen, our results show lower  
295 values compared to Porter’s results, but they are in better agreement with the com-  
296 prehensive set of surveyed excitation cross sections by Majeed and Strickland [81].

297 The total and partial cross sections for nitrogen obtained in the present study  
298 are compared with Grosswendt’s results (dash-dot lines in Fig. 5), whose models are  
299 extensively described in [82, 83, 84]. TCSs are in good agreement with each other  
300 for energies higher than 1 keV, although the individual contributions of different pro-  
301 cesses are different. Grosswendt employs the non-relativistic version of the RBEB,  
302 which leads to an underestimation of the ionization cross section at high energies,  
303 and an empirical screened Rutherford formula to describe the elastic process. The  
304 excitation cross section used by Grosswendt is based on the formulas and cross section  
305 parameters of Porter et al. They introduced modifications to Porter’s parameter to  
306 enhance excitation cross sections across the entire energy range, aiming to improve  
307 agreement with experimental TCS measurements. In line with this goal, they incor-  
308 porated an extra excitation contribution to the cross section shape, which results in  
309 the 20 eV peak [82]. It is worth noting that the Grosswendt’s cross-sections for  $N_2$ ,  
310 already used in the PTra code developed at PTB, have recently been implemented in  
311 the Geant4-DNA toolkit [85].

312 The comparison of our results with other TCS experimental data and theoretical  
313 calculations demonstrates an overall good agreement. However, it is important to  
314 highlight some additional considerations. Firstly, the RBEB model employed in this  
315 study tends to overestimate the ionization cross section, particularly at lower energies  
316 and near the peak. This overestimation may arise from the approximation used, which  
317 does not account for differential oscillator strengths, as previously discussed by Bug  
318 et al. [84]. Secondly, the contribution of the excitation cross section also introduces  
319 a degree of uncertainty. For nitrogen, Itikawa does not provide recommended cross  
320 sections for the excitation of higher allowed states (i.e., those with thresholds above  
321 12.5 eV), which exhibit large cross sections even at high electron energies. Due to  
322 the limited availability of measured values, the Rydberg cross section is also a major  
323 source of uncertainty. Lastly, it is important to note that most of the recommended  
324 data for forbidden excitation processes have large uncertainties, typically ranging  
325 from 25% to 40%. This reflects significant differences in the differential cross sections  
326 measured by different research groups.



(a) N<sub>2</sub>



(b) O<sub>2</sub>

Figure 5: Cross section for electrons in nitrogen (a) and oxygen (b) plotted as a function of electron incident energy for elastic scattering (green), electron excitation (blue), ionization (red), and total (black). The results obtained in the present study for excitation, elastic, ionization and total cross section are presented in solid lines. These are compared with values from Grosswendt and Pszozna [82], Porter et al. [47], Majeed and Strickland [81], Itikawa [45, 46], Williard et al. [86], Garcia and Blanco [79], Iga et al. [69], Shyn et al. [65, 58], Bromberg [63], Daimon et al.[71], and Rapp and Englander-Golden [87].

327 *3.2. Stopping power*

328 To test the consistency of the presented interaction cross sections, we evaluated  
 329 the electron stopping power from the analytical cross sections' models.

330 Assuming that an electron of initial energy  $E$  loses its energy only through exciting  
 331 and ionising collisions, the analytical mass stopping power can be written as

$$-(dE/dx) = -(dE/dx)^{ion} - (dE/dx)^{ex} \quad (10)$$

332 where the pathlength increment  $dx$  is expressed in mass units (i.e., in  $g/cm^2$  ).

333 The first term is given by

$$-(dE/\rho dx)^{ion} = n/\rho \sum_i \int_{B_i}^{(E+B_i)/2} W \frac{d\sigma_i^{ion}}{dW}(E) dW \quad (11)$$

334 where  $\frac{d\sigma_i^{ion}}{dW}(E)$  is the energy-loss cross section for the  $i$ -th ionization shell (with  
 335  $B_i$  its binding energy) for an incident electron of energy  $E$  losing an energy equal to  
 336  $W$  per unit of length,  $\rho$  is the density of the traversed medium and  $n$  is the number  
 337 of molecules per unit of volume. For the second term of the stopping power, which is  
 338 due to electronic excitations of the target, we have

$$-(dE/\rho dx)^{ex} = n/\rho \sum_i \sigma_i^{ex}(E) W_i \quad (12)$$

339 where  $\sigma_i^{ex}(E)$  and  $W_i$  are the excitation cross section and the excitation threshold  
 340 energy for the  $i$ -th electronic excited state of the target, respectively. By substituting  
 341 in Eq. 11-12 the forms of cross sections presented in the previous paragraph (Eq.  
 342 1-7-8), the electron stopping power was calculated in the incident energy range from  
 343 10 eV to 1 MeV.

344 In Figure 6 (a), the calculated mass stopping power values for nitrogen are pre-  
 345 sented. These values are compared with the semi-empirical formula of Peterson and  
 346 Green [89], the Gümüş model [90], and the values from the NIST ESTAR database  
 347 [88], based on ICRU report 37 [21]. For energies higher than 30 eV, the results show  
 348 agreement within 10% with the data predicted by Peterson and Green, as well as  
 349 those by Majeed and Strickland. It should be noted that our results slightly over-  
 350 estimate the stopping power in comparison to the NIST values. This discrepancy is  
 351 likely due to the RBEB model overestimating the impact ionization cross sections,  
 352 in contrast to the recommended values by Itikawa (as discussed in Bug et al. [84]).  
 353 Nevertheless, the agreement between our results and the NIST values remains good,  
 354 with differences within 6% across the entire energy range. For energies lower than 30  
 355 eV there seems to be a lack of contribution to energy loss. To improve the agreement,  
 356 a few corrections and extensions to electronic excitation states could be applied, as  
 357 discussed by Grosswendt et al. [82].

358 In Figure 6 (b), the mass stopping power values for oxygen are compared with

359 Peterson and Green’s semi-empirical formula, Gümüş’s model [90], Gupta’s results  
360 [91], energy loss measurements from Majeed [81], and values from NIST’s ESTAR  
361 database. A very good agreement is observed with the recommended values by NIST,  
362 with relative differences of 3.5% across the entire energy range. As for the other stop-  
363 ping power data, better agreement is obtained with Gupta and Majeed’s predictions,  
364 showing relative differences of about 5% for energies ranging from 30eV to 1 keV,  
365 and less than 10% for higher energies. It could be noted that the calculated stop-  
366 ping power is significantly underestimated for energies below 20-30 eV, and the same  
367 consideration made in the case of nitrogen could be applied.

368 The stopping power values obtained by Gumus are in good agreement with the  
369 intermediate and high energy data in the ESTAR database and seems to better re-  
370 produce energy loss in the very low energy range, given also the good agreement with  
371 Peterson’s results. Nevertheless, Gumus’ model is not derived from cross-section mod-  
372 els but is based on a modified version of Rohrlich and Carlson’s formula for collision  
373 stopping power [92, 93]. This makes it inapplicable for simulation purposes. In this  
374 context, the results obtained with the proposed models in the analysed energy range  
375 represent an excellent set of cross sections to be used for Monte Carlo applications.

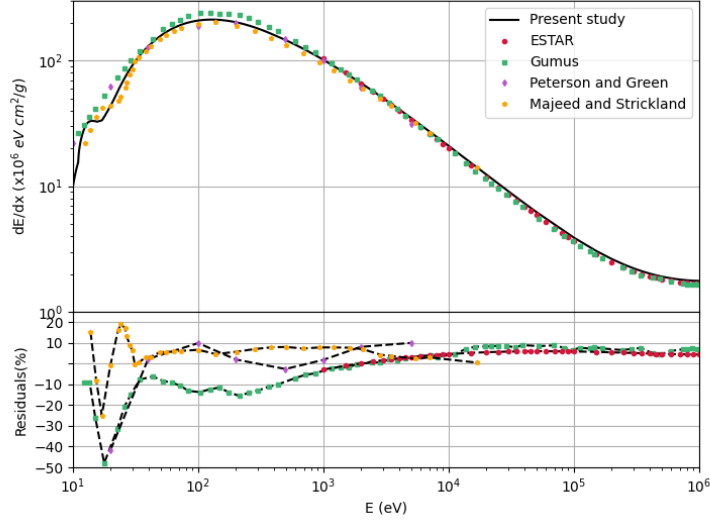
376

#### 377 4. Conclusions and perspectives

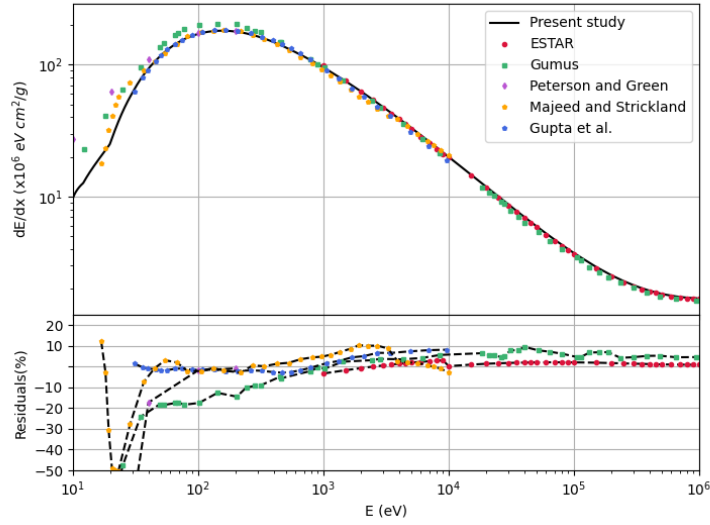
378 The ions produced by cosmic rays in different ionization states and spatial dis-  
379 tribution can significantly change chemical reaction rates by orders of magnitude.  
380 Physics models for electron impact on oxygen and nitrogen molecules to be used in  
381 event-by-event Monte Carlo simulations are a necessary starting point to calculate the  
382 ionization state, the concentration and the spatial distribution of the ions produced  
383 by cosmic rays interaction with molecules in the atmosphere. In this paper, we have  
384 presented models (elastic scattering, electronic excitation and ionization processes)  
385 for electron transport in molecular oxygen and nitrogen that are applicable over a  
386 wide energy range (10 eV - 1 MeV).

387 We evaluated these cross section models by comparing them with experimental  
388 data, obtaining an overall good agreement. A second validation was performed by  
389 comparing the analytically calculated stopping power with values from the NIST  
390 database and from other calculation methodologies. The good agreement of the  
391 stopping power results demonstrates the applicability of the cross-section models  
392 across the entire energy range studied here.

393 Further work is underway to exploit these new cross sections in Monte Carlo  
394 code using a Track-Structure approach for simulation applications. Specifically, we  
395 are working on integrating these models into Geant4-DNA to simulate the ioniza-  
396 tion effects in small volumes at different altitudes in the Earth’s troposphere and  
397 stratosphere.



(a)  $N_2$



(b)  $O_2$

Figure 6: Energy dependence of the electronic mass stopping power in nitrogen (a) and oxygen (b) calculated using Eq. 10. Present calculations (solid black line) are compared with semi-empirical formula of Peterson and Green (purple) [89], Gümüş model (green) [90], semi-empirical formula from Gupta et al. (blue) [91], energy loss measurements from Majeed and Strickland [81], and data from NIST ESTAR database (red) [88]. The relative differences between present analytical results and the other data is shown in the bottom panel of the two figures.

398 The extension of Geant4-DNA to simulate physics for any molecule of climato-  
399 logical interest opens up for the first time the possibility to accurately simulate the  
400 complicated physicochemical processes involved in the atmosphere. Besides atmo-  
401 spheric applications, having a complete set of low-energy electromagnetic interactions  
402 with gaseous molecules may also be of great interest for various applications such as  
403 modeling discharge phenomena, radiation chemistry, micro and nano dosimetry ex-  
404 periments, and exobiology studies.

## Acronyms

**NIST** National Institute of Standards and Technology  
**ICRU** International Commission on Radiation Units and Measurements  
**ESTAR** Stopping Powers and Ranges for Electrons  
**MC** Monte Carlo  
**MC-TS** Monte Carlo Track Structure  
**Geant4** GEometry ANd Tracking  
**RBE** Relativistic Binary Encounter Bethe  
**IAM** Independent Atom Model  
**AR** Additivity Rule  
**SCAR** Screening Corrected Additivity Rule  
**ELSEPA** Elastic Scattering of Electrons and Positrons by neutral Atoms  
**TCS** Total Cross Section  
**DCS** Differential Cross Section

## Acknowledgments

This project has been partially funded by Programma Operativo Nazionale (PON) “Ricerca e Innovazione” 2014–2020 (Decree 1061/2021) Action IV.5 ”Dottorati su tematiche Green”

## References

- [1] Burkholder JB, Abbatt JPD, Barnes I, Roberts JM, Melamed ML, Ammann M, Bertram AK, Cappa CD, Carlton AG, Carpenter LJ, et al. The Essential Role for Laboratory Studies in Atmospheric Chemistry Environ Sci Technol 2017;51:2519–2528 - <https://doi.org/10.1021/acs.est.6b04947>.
- [2] Futrell JH, Tiernan TO. Ion-Molecule Reactions. Science 1968;162(3852):415–422. doi: 10.1126/science.162.3852.415.
- [3] Kinetic Database for Astrochemistry: KIDA. <https://kida.astrochem-tools.org/>

- [4] Satta M, Castrovilli MC, Nicolanti F, Casavola AR, Mancini TC, Cartoni A. Perspectives of Gas Phase Ion Chemistry: Spectroscopy and Modeling. *Condensed Matter*. 2022;7(3):46. <https://doi.org/10.3390/condmat7030046>.
- [5] Cartoni A, Catone D, Bolognesi P, Satta M, Markus P, Avaldi L.  $\text{HSO}_2^+$  formation from ion-molecule reactions of  $\text{SO}_2^+$  with water and methane: two fast reactions with reverse temperature-dependent kinetic trend. *HOT Paper Chem Eur J* 2017;23:6772-6780. <https://doi.org/10.1002/chem.201700028>.
- [6] Satta M, Cartoni A, Catone D, Castrovilli MC, Bolognesi P, Zema N, Avaldi L. The reaction of sulfur dioxide radical cation with hydrogen and its relevance in solar geoengineering models. *ChemPhysChem* 2020;21:1146-1156. <https://doi.org/10.1002/cphc.202000194>.
- [7] Ravishankara AR, Daniel JS, Portmann RW. Nitrous oxide ( $\text{N}_2\text{O}$ ): the dominant ozone-depleting substance emitted in the 21st century. *Science* 2009;326(5949):123-125. doi: 10.1126/science.1176985.
- [8] Portmann RW, Daniel JS, Ravishankara AR. Stratospheric ozone depletion due to nitrous oxide: influences of other gases. *Philos Trans R Soc Lond B Biol Sci* 2012;367(1593):1256-64. doi: 10.1098/rstb.2011.0377.
- [9] Müller R. The impact of the rise in atmospheric nitrous oxide on stratospheric ozone. *Ambio* 2021;50(1):35-39. <https://doi.org/10.1007/s13280-020-01428-3>.
- [10] Incerti S, Kyriakou I, Bernal MA, Bordage MC, Francis Z, Guatelli S, Ivanchenko V, Karamitros M, Lampe N, Lee SB et al. Geant4-DNA example applications for track structure simulations in liquid water: A report from the Geant4-DNA Project. *Med Phys* 2018;45:e722-e739. <https://doi.org/10.1002/mp.13048>.
- [11] Bernal MA, Bordage MC, Brown JMC, Davidková M, Delage E, El Bitar Z, Enger SA, Francis Z, Guatelli S, Ivanchenko VN, et al. Track structure modeling in liquid water: A review of the Geant4-DNA very low energy extension of the Geant4 Monte Carlo simulation toolkit. *Phys Med* 2015;31:861-874. <https://doi.org/10.1016/j.ejmp.2015.10.087>.
- [12] Incerti S, Baldacchino G, Bernal M, Capra R, Champion C, Francis Z, Guatelli S, Guèye P, Mantero A, Mascialino B et al. The Geant4-DNA project. *Int J Model Simul Sci Comput* 2010;1:157-178. <https://doi.org/10.48550/arXiv.0910.5684>.
- [13] Incerti S, Ivanchenko A, Karamitros M, Mantero A, Moretto P, Tran HN, Mascialino B, Champion C, Ivanchenko VN, Bernal MA et al. Comparison of Geant4 very low energy cross section models with experimental data in water. *Med Phys* 2010;37:4692-4708. <http://dx.doi.org/10.1118/1.3476457>.

- [14] Agostinelli S et al. GEANT4 - A Simulation Toolkit. Nucl Instrum Methods A 2003;506:250-303. [https://doi.org/10.1016/S0168-9002\(03\)01368-8](https://doi.org/10.1016/S0168-9002(03)01368-8).
- [15] Allison J et al. Geant4 Developments and Applications. IEEE Transactions on Nuclear Science 2006;53:270-278. <https://doi.org/10.1109/TNS.2006.869826>.
- [16] Allison J et al. Recent Developments in GEANT4. Nucl Instrum Methods A 2016;835:186-225. <https://doi.org/10.1016/j.nima.2016.06.125>.
- [17] Shin WG, Ramos-Mendez J, Tran NH, Okada S, Perrot Y, Villagrasa C, Incerti S. Geant4-DNA simulation of the pre-chemical stage of water radiolysis and its impact on initial radiochemical yields. Phys Med 2021;88:86-90. <https://doi.org/10.1016/j.ejmp.2021.05.029>
- [18] Chappuis F, Grilj V, Tran HN, Zein SA, Bochud F, Bailat C, Incerti S, Desorgher L. Modeling of scavenging systems in water radiolysis with Geant4-DNA. Phys Med 2023;108:102549. <https://doi.org/10.1016/j.ejmp.2023.102549>.
- [19] Hoyle CR, Fuchs C, Järvinen E, Saathoff H, Dias A, El Haddad I, Gysel M, Coburn SC, Tröstl J, Bernhammer AK, Bianchi F, Breitenlechner M, Corbin JC, Craven J, Donahue NM, Duplissy J, Ehrhart S, Frege C, Gordon H, Höppel N, Heinritzi M, Kristensen TB, Molteni U, Niehman L, Pinterich T, Prévôt ASH, Simon M, Slowik JG, Steiner G, Tomé A, Vogel AL, Volkamer R, Wagner AC, Wagner R, Wexler AS, Williamson C, Winkler PM, Yan C, Amorim A, Dommen J, Curtius J, Gallagher MW, Flagan RC, Hansel A, Kirkby J, Kulmala M, Möhler O, Stratmann F, Worsnop DR, Baltensperger U. Aqueous phase oxidation of sulphur dioxide by ozone in cloud droplets. Atm Chem Phys 2016;16:1693–1712. <https://doi.org/10.5194/acp-16-1693-2016>.
- [20] Voigtländer J, Duplissy J, Rondo L, Kürten A, Stratmann F. Numerical simulations of mixing conditions and aerosol dynamics in the CERN CLOUD chamber. Atm Chem Phys 2012;12(4);2205-2214. <https://doi.org/10.5194/acp-12-2205-2012>.
- [21] ICRU, "Stopping powers for electrons and positrons," Report No. 37, International Commission on Radiation Units and Measurements, Bethesda, MD, 1984. <http://dx.doi.org/10.1093/jicru/os19.2.Report37>
- [22] Kim Y, Santos J, Parente F. Extension of the Binary-Encounter-Dipole Model to Relativistic Incident Electrons. Phys Rev 2000;A62:052710. <https://doi.org/10.1103/PhysRevA.62.052710>.
- [23] Kim YK, Rudd ME. Binary-encounter-dipole model for electron-impact ionization. Phys Rev 1994;A50:3954–3967. <http://dx.doi.org/10.1103/PhysRevA.50.3954>.

- [24] Tessaro VB, Gervaisc B, Poignantb F, Beuveb M, Galassi ME. Monte Carlo transport of swift protons and light ions in water: The influence of excitation cross sections, relativistic effects, and Auger electron emission in w-values. *Phys Med* 2021;88:71-85. <https://doi.org/10.1016/j.ejmp.2021.06.006>.
- [25] Kim YK. Total Ionization Cross Sections of Molecules by Electron Impact. In: Christophorou, L.G., Olthoff, J.K., Vassiliou, P. (eds) *Gaseous Dielectrics X*, . Springer, Boston, MA, 2004. [https://doi.org/10.1007/978-1-4419-8979-6\\_1](https://doi.org/10.1007/978-1-4419-8979-6_1)
- [26] Hwang W, Kim YK, Rudd ME. New model for electron impact ionization cross sections of molecules. *J Chem Phys* 1996;104:2956. <https://doi.org/10.1063/1.471116>.
- [27] Santos JP et al. Cross sections for K-shell ionization of atoms by electron impact. *J Phys B: At Mol Opt Phys* 2003;36:4211. <https://dx.doi.org/10.1088/0953-4075/36/21/002>.
- [28] Edel S. Modelisation du Transport des Photons et de s'Electrons Dans l'ADN Plasmide. PhD Thesis, Universite Toulouse III-Paul Sabatier, Toulouse, France, 2006. <https://theses.hal.science/tel-01998577/document>.
- [29] Hwang W, Kim YK, Rudd ME. New model for electron-impact ionization cross sections of molecules. *J Chem Phys* 1996;104:2956–66. <http://dx.doi.org/10.1063/1.471116>.
- [30] Jolly WL, Bomben KD, Eyermann CJ. Core-electron binding energies for gaseous atoms and molecules. *At Data Nucl Data Tables* 1984;31:411. [https://doi.org/10.1016/0092-640X\(84\)90011-1](https://doi.org/10.1016/0092-640X(84)90011-1).
- [31] Massey HSW, Burhop EHS, Gilbody HB. *Atomic Scattering: Electronic and Ionic Impact Phenomena*. Second Edition, 1969, Vol.2. <https://www.science.org/doi/10.1126/science.168.3930.462.b>.
- [32] Blanco F, García G. Screening corrections for calculation of electron scattering from polyatomic molecules. *Phys Lett A* 2003;317:458. <https://doi.org/10.1016/j.physleta.2003.09.016>.
- [33] Blanco F, García G. Screening corrections for calculation of electron scattering differential cross sections from polyatomic molecules. *Phys Lett A* 2004;330:230. <https://doi.org/10.1016/j.physleta.2004.07.027>.
- [34] Sanz AG, Fuss MG, Blanco F, Gorfinkiel JD, Almeida D, Ferreira da Silva F, Limão-Vieira P, Brunger MJ, García G. An investigation into electron scattering from pyrazine at intermediate and high energies. *J Chem Phys* 2013;139:184310. <http://dx.doi.org/10.1063/1.4829771>

- [35] Milosavljević AR et al. Absolute cross sections for elastic electron scattering from 3-hydroxytetrahydrofuran. *New J Phys* 2008;10:103005. doi:10.1088/1367-2630/10/10/103005
- [36] Maljkovic JB, Milosavljevic AR, Blanco F, Šević D, García G, Marinkovic BP. *Phys Rev* 2009;A79:052706. <https://doi.org/10.1103/PhysRevA.79.052706>
- [37] Blanco F, García G. Screening corrections for calculation of electron scattering from polyatomic molecules. *Phys Lett* 2003;A317:458–462. <https://doi.org/10.1016/j.physleta.2004.07.027>
- [38] Fuss MC, Sanz AG, Blanco F, Limão-Vieira P, Brunger MJ, García G. Differential and integral electron scattering cross sections from tetrahydrofuran (THF) over a wide energy range: 1-10000 eV. *Eur Phys J D* 2014;68(6). <https://www.researchgate.net/publication/273568027>
- [39] Raj D. A note on the use of the additivity rule for electron-molecule elastic scattering. *Phys Lett A* 1991;160:6-9. [https://doi.org/10.1016/0375-9601\(91\)91070-T](https://doi.org/10.1016/0375-9601(91)91070-T)
- [40] Blanco F, Ellis-Gibbins L, García G. Screening corrections for the interference contributions to the electron and positron scattering cross sections from polyatomic molecules, *Chem Phys Lett* 2016;64571-75. <https://doi.org/10.1016/j.cplett.2015.11.056>.
- [41] Salvat F, Jablonski A, Powell CJ. ELSEPA—Dirac partial-wave calculation of elastic scattering of electrons and positrons by atoms, positive ions and molecules. *Comput Phys Commun* 2005;165:157–190. <https://doi.org/10.1016/j.cpc.2020.107704>.
- [42] Demes S, Kelemen V, Remeta EY. Elastic electron scattering by the CF<sub>3</sub> radical in the 1–1000 eV energy range. *J Phys B: At Mol Opt Phys* 2017;50(13):135201. <https://dx.doi.org/10.1088/1361-6455/aa739f>
- [43] PubChem, PubChem Database (2019), <https://pubchem.ncbi.nlm.nih.gov>.
- [44] Computational Chemistry Comparison and Benchmark DataBase Release 22 (May 2022) Standard Reference Database 101. <https://cccbdb.nist.gov/pollistx.asp>
- [45] Itikawa Y. Cross Sections for Electron Collisions with Oxygen Molecules. *J Phys Chem Ref Data* 2009;38(1):1–20. <https://doi.org/10.1063/1.3025886>
- [46] Itikawa Y. Cross Sections for Electron Collisions with Nitrogen Molecules. *J Phys Chem Ref Data* 2006;35(1):31–53. <http://dx.doi.org/10.1063/1.1937426>

- [47] Porter HS, Jackman CH, Green AES. Efficiencies for production of atomic nitrogen and oxygen by relativistic proton impact in air. *J Chem Phys* 1976;65:154. <http://dx.doi.org/10.1063/1.432812>
- [48] Green AES, Stolarski RS. Analytic models of electron impact excitation cross sections. *J Atm Terrest Phys* 1972;54:1703-1717. [http://dx.doi.org/10.1016/0021-9169\(72\)90030-X](http://dx.doi.org/10.1016/0021-9169(72)90030-X)
- [49] Stolarski RS, Green AES. Calculations of auroral intensities from electron impact. *J Geophys Res* 1967;72(15):3967-3974. <https://doi.org/10.1029/JZ072i015p03967>
- [50] Watson CE, Dulock VA, Stolarski RS, Green AES. Electron impact cross sections for atmospheric species: 3. Molecular oxygen. *J Geophys Res* 1967;72(15):3961-3966. <https://doi.org/10.1029/JZ072i015p03961>
- [51] Opal CB, Beaty EC, Peterson WK. Tables of secondary-electron-production cross sections. *At Data* 1972;4:209-253. [https://doi.org/10.1016/S0092-640X\(72\)80004-4](https://doi.org/10.1016/S0092-640X(72)80004-4)
- [52] Shyn TW, Sharp WE. Doubly differential cross sections of secondary electrons ejected from molecular oxygen by electron impact. *Phys Rev A* 1991;43(5):2300-2305. <https://doi.org/10.1103/PhysRevA.43.2300>
- [53] Shyn TW. Doubly differential cross sections of secondary electrons ejected from gases by electron impact: 50-400 eV on N<sub>2</sub>. *Phys Rev A* 1983;27(5):2388-2395. <https://doi.org/10.1103/PhysRevA.27.2388>
- [54] DuBois RD, Rudd ME. Absolute doubly differential cross sections for ejection of secondary electrons from gases by electron impact. II. 100-500-eV electrons on neon, argon, molecular hydrogen, and molecular nitrogen. *Phys Rev A* 1978;17(3):843-848. <https://doi.org/10.1103/PhysRevA.17.843>
- [55] Pal S, Kumar J, Bhatt P. Electron impact ionization cross-sections for the N<sub>2</sub> and O<sub>2</sub> molecules. *Journal of Electron Spectroscopy and Related Phenomena* 2003;129(1):35-41. [https://doi.org/10.1016/S0368-2048\(03\)00033-1](https://doi.org/10.1016/S0368-2048(03)00033-1)
- [56] Jain DK, Khare SP. Ionizing collisions of electrons with CO<sub>2</sub>, CO, H<sub>2</sub>O, CH<sub>4</sub> and NH<sub>3</sub>. *J Phys B: At Mol Opt Phys* 1976;9(8):1429-1438. <https://dx.doi.org/10.1088/0022-3700/9/8/023>
- [57] Gote M, Ehrhardt H. Rotational excitation of diatomic molecules at intermediate energies: absolute differential state-to-state transition cross sections for electron scattering from N<sub>2</sub>, Cl<sub>2</sub>, CO and HCl. *J Phys B: At Mol Opt Phys* 1995;28:3957. <https://dx.doi.org/10.1088/0953-4075/28/17/029>

- [58] Shyn TW, Carignan GR. Angular distribution of electrons elastically scattered from gases: 1.5-400 eV on N<sub>2</sub>. Phys Rev A 1980;22(3):923–929. <https://doi.org/10.1103/PhysRevA.22.923>
- [59] Srivastava SK, Chutjian A, Trajmar S. Absolute elastic differential electron scattering cross sections in the intermediate energy region. II.— N<sub>2</sub>. J Chem Phys 1976;64:1340. <https://doi.org/10.1063/1.432400>
- [60] Nickel JC, Mott C, Kanik I, McCollum DC. Absolute elastic differential electron scattering cross sections for carbon monoxide and molecular nitrogen in the intermediate energy region. J Phys B: At Mol and Opt Phys 1988;21(10):1867–1877. <https://doi.org/10.1088/0953-4075/21/10/018>.
- [61] Jansen RHJ, Heer FJ, Luyken HJ, Wingerden B, Blaauw HJ. Absolute differential cross sections for elastic scattering of electrons by helium, neon, argon and molecular nitrogen. J Phys B: At Mol and Opt Phys 1976;9(2):185–212. <https://doi.org/10.1088/0022-3700/9/2/009>.
- [62] Herrmann D. Differential cross sections for elastic electron scattering. II. Charge cloud polarization in N<sub>2</sub>. J Chem Phys 1976;64(1). <https://doi.org/10.1063/1.431951>.
- [63] Bromberg JP. Absolute Differential Cross Sections of Elastically Scattered Electrons. I. He, N<sub>2</sub>, and CO at 500 eV. J Chem Phys 1969;50(9):3906. <http://dx.doi.org/10.1063/1.1671647>.
- [64] Linert I, King GC, Zubek M. Measurements of differential cross sections for elastic electron scattering in the backward direction by molecular oxygen. J Phys B: At Mol and Opt Phys 2004;37(23):4681–4691. <https://dx.doi.org/10.1088/0953-4075/37/23/009>.
- [65] Shyn TW, Sharp WE. Angular distribution of electrons elastically scattered from O<sub>2</sub>: 2.0-200 eV impact energy. Phys Rev A 1982;26(3):1369. <https://doi.org/10.1103/PhysRevA.26.1369>.
- [66] Trajmar S, Cartwright D, Williams W. Differential and Integral Cross Sections for the Electron-Impact Excitation of the  $a^1\Delta_g$  and  $b^1\Sigma_g^+$  States of O<sub>2</sub>. Phys Rev A 1971;4(4):1482–1492. <https://doi.org/10.1103/PhysRevA.4.1482>.
- [67] Woste G. et al. Differential and integral cross sections for elastic scattering of low-energy electrons by O<sub>2</sub>. J Phys B: At Mol Opt Phys 1995;28:4141. <https://dx.doi.org/10.1088/0953-4075/28/18/016>.
- [68] Sullivan JP, Gibson JC, Gulley RJ, Buckman SJ. Low-energy electron scattering from O<sub>2</sub>. J. Phys. B: At. Mol. Opt. Phys. 1995;28:4319. DOI: 10.1088/0953-4075/28/19/017

- [69] Iga I et al. Elastic differential cross section measurements for electron scattering from Ar and O<sub>2</sub> in the intermediate-energy range. *J Phys B: Atom Mol Phys* 1987;20:1095. <https://dx.doi.org/10.1088/0022-3700/20/5/025>.
- [70] Bromberg JP Absolute differential cross sections of elastically scattered electrons. V. O<sub>2</sub> and CO<sub>2</sub> at 500, 400, and 300 eV. *J Chem Phys* 1974;60(5):1717. <https://doi.org/10.1063/1.1681265>.
- [71] Daimon H, Hayashi S, Kondow T, Kuchitsu K. Measurements of Differential Cross Sections of Low-Energy Electrons Elastically Scattered by Gas Molecules. II. Scattering of 200–500 eV Electrons by Molecular Oxygen. *Journal of the Physical Society of Japan* 1982;51(8):2641–2649. <https://doi.org/10.1143/JPSJ.51.2641>.
- [72] Lxcat. LXCat website, <https://nl.lxcat.net/contributors/>
- [73] Biagi SF. Monte Carlo simulation of electron drift and diffusion in counting gases under the influence of electric and magnetic fields. *Nucl Instrum Meth A* 1999;421(1-2):234-240. [https://doi.org/10.1016/S0168-9002\(98\)01233-9](https://doi.org/10.1016/S0168-9002(98)01233-9).
- [74] Wakiya K. Differential and integral cross sections for the electron impact excitation of O<sub>2</sub>. I. Optically allowed transitions from the ground state. *J Phys B: Atom Mol Phys* 1978;11:3913. <https://dx.doi.org/10.1088/0022-3700/11/22/019>.
- [75] Trajmar S, Williams W, Kuppermann A. Angular Dependence of Electron Impact Excitation Cross Sections of O<sub>2</sub>. *J Chem Phys* 1972;56:3759. <https://doi.org/10.1063/1.1677774>.
- [76] Linder F, Schmidt H. Experimental Study of Low Energy e-O<sub>2</sub> Collision Processes. *Zeitschrift für Naturforschung A* 1971;26(10):1617-1625. <https://doi.org/10.1515/zna-1971-1008>.
- [77] Kim YK. Scaling of plane-wave Born cross sections for electron-impact excitation of neutral atoms. *Phys Rev A* 2001;64(3):032713. <https://doi.org/10.1103/PhysRevA.64.032713>.
- [78] Suzuki D, Kato H, Ohkawa M, Anzai K, Tanaka H, Limao-Vieira P, Campbell L, Brunger MJ. Electron excitation of the Schumann–Runge continuum, longest band, and second band electronic states in O<sub>2</sub>. *J Chem Phys* 2011;134(6):064311. <https://doi.org/10.1063/1.3533442>.
- [79] García G, Blanco F. Energy dependence of the total cross section for electron scattering by N<sub>2</sub> and CO molecules at energies above 1 keV. *Phys Lett A* 2001;279:1–2. [https://doi.org/10.1016/S0375-9601\(00\)00822-7](https://doi.org/10.1016/S0375-9601(00)00822-7)

- [80] Brunger MJ, Thorn PA, Campbell L, Kato H, Kawahara H, Hoshino M, Tanaka H, Kim YK. Application of the BEf-scaling approach to electron impact excitation of dipole-allowed electronic states in molecules. *J Phys: Conference Series* 2008;115:012004. <https://dx.doi.org/10.1088/1742-6596/115/1/012004>.
- [81] Majeed T, Strickland DJ. New survey of Electron Impact Cross Sections for Photoelectron and Auroral Electron Energy Loss Calculations. *J Phys Chem Ref Data* 1997;26:335-349. <https://doi.org/10.1063/1.556008>.
- [82] Grosswendt B, Pszona S. The track structure of  $\alpha$ -particles from the point of view of ionization-cluster formation in nanometric volumes of nitrogen. *Radiat Environ Biophys* 2002;41(2):91–102. <http://dx.doi.org/10.1007/s00411-002-0144-9>.
- [83] Grosswendt B, Waibel E. Transport of low energy electrons in nitrogen and air. *Nucl Instrum Methods* 1978;155(1–2):145–56. [http://dx.doi.org/10.1016/0029-554X\(78\)90198-2](http://dx.doi.org/10.1016/0029-554X(78)90198-2).
- [84] Bug M, Gargioni E, Nettelbeck H, Baek W, Hilgers G, Rosenfeld A et al. Ionization cross section data of nitrogen, methane, and propane for light ions and electrons and their suitability for use in track structure simulations. *Phys Rev E* 2013;88(4). <http://dx.doi.org/10.1103/PhysRevE.88.043308>.
- [85] Pietrzak M. et al. Intercomparison of nanodosimetric distributions in nitrogen simulated with Geant4 and PTra track structure codes. *Phys Med* 2022;102:103-109. <https://doi.org/10.1016/j.ejmp.2022.09.003>.
- [86] Williard A, Kendall PA, Blanco F, Tegeder P, Garcia G, Mason NJ. Inelastic scattering and stopping power for electrons in O<sub>2</sub> and O<sub>3</sub> at intermediate and high energies, 0.3–5 keV. *Chem Phys Lett* 2003;375:39–44. [https://doi.org/10.1016/S0009-2614\(03\)00801-7](https://doi.org/10.1016/S0009-2614(03)00801-7).
- [87] Rapp D, Englander-Golden P. Total Cross Sections for Ionization and Attachment in Gases by Electron Impact. I. Positive Ionization. *J Chem Phys* 1965;43:1464. <https://doi.org/10.1063/1.1696957>.
- [88] NIST. ESTAR database, URL <https://physics.nist.gov/PhysRefData/Star/Text/ESTAR.html>.
- [89] Peterson LR, Green AES. The relation between ionization yields, cross sections and loss functions. *J Phys B* 1968;1:1131–1140. DOI 10.1088/0022-3700/1/6/317
- [90] Gumus H. Simple stopping power formula for low and intermediate energy electrons. *Rad Phys Chem* 2005;72:7–12. <http://dx.doi.org/10.1016/j.radphyschem.2004.03.006>.

- [91] Gupta P, Jhanwar BL, Khare SP. Stopping power of atmospheric gases for electrons. *Physica B+C* 1975;79B:311-321. [https://doi.org/10.1016/0378-4363\(75\)90098-4](https://doi.org/10.1016/0378-4363(75)90098-4).
- [92] Rohrlich F, Carlson BC. Positron-electron differences in energy loss and multiple scattering. *Phys Rev* 1954;93:38-44. <https://doi.org/10.1103/PhysRev.93.38>.
- [93] Sugiyama H. Stopping power formula for intermediate energy electrons. *Phys Med Biol* 1985;30:4331-4335. <https://doi.org/10.1016/j.radphyschem.2004.03.006>